ELSEVIER

Journal of Nuclear Materials 240 (1997) 205–214

journal of nuclear materials

A generalized model for radiation-induced amorphization and crystallization of U_3Si and U_3Si_2 and recrystallization of UO_2 [1]

J. Rest *

Energy Technology Division, Argonne National Laboratory, Argonne, IL 60439, USA

Received 10 June 1996; accepted 15 October 1996

Abstract

A rate-theory model of radiation-induced amorphization and crystallization of U_3Si during ion irradiation has been generalized to include U_3Si_2 and UO_2. The generalized model has been applied to ion-irradiation and in-reactor experiments on U_3Si and U_3Si_2 and provides an interpretation for the amorphization curve (dose required to amorphize the material as a function of temperature), for the ion-radiation-induced nanoscale polycrystallization of these materials at temperatures above the critical temperature for amorphization, as well as for the role of the small crystallites in retarding amorphization. An alternative mechanism for the evolution of recrystallization nuclei is described for a model of irradiation-induced recrystallization of UO_2 wherein the stored energy in the UO_2 is concentrated in a network of sinklike nuclei that diminish with dose due to interaction with radiation-produced defects. The sinklike nuclei are identified as cellular dislocation structures that evolve relatively early in the irradiation period. The complicated kinetics involved in the formation of a cellular dislocation network are approximated by the formation and growth of subgrains due to the interaction of shock waves produced by fission-induced damage to the UO_2.

1. Introduction

A rate-theory model [1] for ion-induced crystallization and amorphization of U_3Si has been generalized to include U_3Si_2 and UO_2. The bombardment of solids by energetic particles produces displacements of the host atoms and thus damage to the structure of the solids. If the damage energy is sufficiently high, displacement cascades containing hundreds of atoms each are produced. The early stages of cascade development are characterized by the formation of shock waves [2–7], and, in some materials (e.g., Si, U_3Si, U_3Si_2) amorphous material is left after the cascades cool to ambient temperature [8]. In other materials (such as UO_2), the 'molten' material within the damage cascade crystallizes upon 'cooling.' Within the context of the model, the bombarding ions produce clusters of amorphous material that are considered centers of expansion (CE), or excess free volume zones. Simultaneously, centers of compression (CC) are created in the material. The CCs are local regions of increased density that travel through the material as an elastic (e.g., acoustic) shock wave. The CEs can be annihilated upon contact with a sufficient number of CCs, forming either a crystallized region that is indistinguishable from the host material, or a region with a slight disorientation (crystallized grain). The CCs can also annihilate each other upon contact, forming either oriented or slightly disoriented crystal structures. Crystallized grains grow by accumulating additional CCs. Full amorphization (or full crystallization) is calculated on the basis of achieving a volume fraction consistent with the close packing of spherical entities. The possibility of anti-site defects is not considered here.

The generalized model has been applied to ion-irradiation and in-reactor experiments on U_3Si and U_3Si_2 and

* Tel.: +1-630 252 5026; fax: +1-630 252 4798; e-mail: rest@maat.mct.anl.gov.

[1] Work supported by U.S. Department of Energy, Office of Arms Control and Nonproliferation, under Contract W-31-109-Eng-38.

PII S0022-3115(96)00714-3

provides an interpretation for the amorphization curve (dose required to amorphize the material as a function of temperature), for the ion-radiation-induced nanoscale polycrystallization of these materials at temperatures above the critical temperature for amorphization, as well as for the role of the small crystallites in retarding amorphization.

The peripheral region of UO_2 fuel pellets reveals an increasingly porous microstructure with burnup [9–12]. Observations of this 'rim effect' show that an extremely fine-grained structure formed by recrystallization of the original grains is associated with this porous microstructure. TEM observations [13] of the formation mechanism of the recrystallized region show that dislocation density increases with burnup. Low-angle boundaries begin to form above 7.5 to 8×10^{20} fissions/cm^3. Subdivided grains 20–30 nm in size and with high-angle boundaries due to the accumulation of an extremely high density of subboundaries, together with recrystallized grains 50–200 nm in size and adjacent to the subdivided grain region, are observed in fuel irradiated to 2.1×10^{21} fissions/cm^3.

This is essentially the physical picture that was proposed as the basis of a model for irradiation-induced recrystallization wherein the stored energy in the material is concentrated in a network of sinklike nuclei that diminish with dose due to interaction with radiation-produced defects [14]. The sinklike nuclei are identified as cellular dislocation structures that evolve relatively early in the irradiation period. Impurities formed during fissioning of the material diffuse as vacancy–impurity complexes to cell walls where they effectively pin the wall, i.e., dislocation movement to and from the wall is hindered. The walls containing no impurities continue to undergo subgrain coalescence that results in viable nuclei for recrystallization. Recrystallization is induced when the energy per nucleus is high enough that the creation of grain-boundary surfaces is offset by the creation of strain-free volumes, with a resultant net decrease in the free energy of the material. This formulation was shown to provide a plausible interpretation of the fission density at which grain subdivision begins.

Nevertheless, this physical picture of the processes leading up to recrystallization is qualitative and has eluded a mechanistic description. One of the primary purposes of this paper is to show that a mechanistic description of these prerecrystallization processes, consistent with observation, can be achieved by a utilization of the generalized theory of radiation-induced amorphization and crystallization.

2. Model

Amorphization of a crystallized U_3Si grain is hindered by the presence of the grain boundary. Preirradiation of U_3Si [15] and Zr_3Al [16] above the critical temperature for amorphization results in the observed formation of nanometer-size grains. In addition, the subsequent reradiation of U_3Si samples [15] at temperatures below the critical temperature shows that the material has developed a resistance to radiation-induced amorphization (i.e., a higher dose is needed to amorphize the preirradiated samples than for those that have not been preirradiated). In the model, it is assumed that grain boundaries act as effective defect sinks, and enhanced defect annihilation is responsible for retarding amorphization at low temperature.

The atom fraction of amorphous clusters, C_{ce}, evolves in time according to

$$\frac{dC_{ce}}{dt} = N_{ce}\xi_a K\left(V_O^f + \delta R_g + V_\alpha C_g\right) - f_1\frac{N_{ce}}{N_{cc}}v_a C_{cc}C_{ce} - (f_{ie}K\omega_{ie} + f_t\omega_t)C_{ce}, \quad (1)$$

where K is the damage rate in displacements per atom per second (dpa/s), N_{ce} are N_{cc} the atom fraction of CEs and CCs created per dpa, ξ_a is a measure of the stability of the amorphous clusters formed by the damage cascade (i.e., $\xi_a = 1$ means that all amorphous clusters survive the supercooling of the cascade region), $V_\alpha = V_c N_0$, where V_c is the volume of amorphous material created per N_{ce}; N_0 is the number of atoms per unit volume; V_O^f is the volume fraction of unaltered material; and C_g and R_g are the crystallized grain density and grain radius, respectively. δ provides a measure of the difficulty in amorphizing the boundary region by ion damage ($1/(\delta R_g)$ is a measure of the effective grain boundary area per unit volume), T is the absolute temperature, and Ω is the atomic volume. v_a is given by

$$v_a = v_{cc}e^{-\ a/kT}, \quad (2)$$

where v_{cc} is the velocity of the shock wave in the material, and $_a$ is the activation energy for crystallization of an amorphous cluster by a CC. In addition,

$$\omega_{ie} = e^{-\ ie/kT}, \quad (3a)$$

$$\omega_t = e^{-\ t/kT}, \quad (3b)$$

where $_{ie}$ and $_t$ are the activation energies for irradiation enhanced and thermal crystallization, respectively.

The corresponding equation for the density of the centers of compression, C_{cc}, is given by

$$\frac{dC_{cc}}{dt} = N_{cc}K\left(V_O^f + \delta R_g + V_\alpha C_g\right) - f_1 v_a C_{cc}C_{ce} - f_2 v_x C_{cc}C_g R_g - f_3 v_{cc}C_{cc}C_{cc}, \quad (4)$$

where v_x is given by

$$v_x = v_{cc}e^{-\ x/kT}, \quad (5)$$

where $_x$ is the activation energy for grain growth due to interaction between a CC and a crystallized grain.

The first three terms on the right-hand side (RHS) of Eqs. (1) and (4) represent the gain of CEs and CCs due to production by ion damage in (a) the unaltered solid matrix,

(b) the grain boundary of crystallized grains, and (c) the crystallized grain embryos. The fourth term on the RHS of Eqs. (1) and (4) represents the loss of CEs and CCs due to annihilation of the CEs by CCs. The last two terms in Eq. (1) are the loss of CEs by irradiation-enhanced and thermal dissociation mechanisms, respectively. The last two terms in Eq. (4) represent the loss of CCs due to interaction with crystallized grain nuclei and CC pair annihilation, respectively. Note from the fourth terms on the RHS of Eqs. (1) and (4) that the loss rates of CEs and CCs due to 'recombination' are identical only for the case where $N_{ce} = N_{cc}$ (i.e., for $N_{ce} \neq N_{cc}$ more than 1 CC is needed to annihilate a CE). In general, N_{ce} and N_{cc} are functions of ion energy.

During irradiation amorphous clusters are produced having different shapes and sizes. Eqs. (1) and (4) utilize the assumption that the cluster size distribution can be represented, to first order, by the density of 'average' size spherical clusters. This type of approximation is relatively common in other areas. For example, the radiation produced fission-gas bubble-size distribution is usually represented by the density of 'average' size bubbles [17,18]. Similarly, the ratio of the number of amorphous clusters produced to the number of shock waves produced per ion, N_{ce}, N_{cc} is assumed to be an average 'constant' value. The effects of the variation of this parameter with ion energy are assumed to be of second order.

The time rate of change of the density (in units of atom fraction) of crystallized grains, C_g, is given by

$$\frac{dC_g}{dt} = \beta_1 f_1 \frac{N_{ce}}{N_{cc}} v_a C_{cc} C_{ce} - \beta_3 f_3 v_{cc} C_{cc} C_{cc} - N_{ce} K \xi_g V_\alpha C_g, \tag{6}$$

where β_1 and β_3 are the probabilities that the interaction between a CE and a CC, and between a CC and a CC, respectively, results in a crystallized grain (instead of a resultant atom orientation that is in alignment with the original grain structure). The last term in Eq. (6) corresponds to the third terms on the RHS of Eqs. (1) and (4) and is the loss of crystallized grain nuclei due to amorphization by an incoming ion. ξ_g is the probability that for amorphous clusters which are unstable and recrystallize during the solidification of the cascade (i.e., $\xi < 1$), the nuclei is left intact. The radius of the crystallized grains is given by

$$R_g = \left(\frac{V_g}{4\pi/3} \right)^{1/3}, \tag{7}$$

where

$$V_g = \frac{V_g^f}{C_g}, \tag{8}$$

and

$$\frac{dV_g^f}{dt} = \beta_2 f_2 v_x C_{cc} C_g R_g^2 A_{cc} - \delta R_g N_{ce} K \xi_g V_\alpha. \tag{9}$$

In Eq. (9), β_2 is the probability that an interaction between a CC and a crystallized grain results in the growth of the grain (as compared to formation of a region of the material adjacent to the crystallized grain whose atoms are in alignment with the crystal structure of the host atoms),

$$A_{cc} = 2\pi\left((\eta_{cc}\Omega)/(4\pi/3) \right)^{2/3}$$

is the effective surface area of a CC, and η_{cc} is the fractional density decrease that occurs upon the creation of a CC. In Eq. (9), it is assumed that the interaction between a CC and a crystallized grain can be described by the Gibbs theory of surfaces. The first term of Eq. (9) describes the growth of crystallized grains by accumulation of CCs. The last term in Eq. (9) corresponds to the second terms on the RHS of Eqs. (1) and (4) and is the loss of crystallized grain volume due to amorphization by an incoming ion.

It is assumed here that interaction between the CEs, the CCs, and crystallized grains is facilitated by the presence of radiation-produced. Thus the rate constants, f_1–f_3, include not only the standard interaction cross sections, but the probability of finding an appropriate number of radiation-produed defects in the near vicinity of the interaction site.

It is also assumed that N_{ce} and N_{cc} are not independent, but are related by the volume change, ΔV, in the material due to amorphization. If it is assumed that a CE results in an average fractional density increase η_{ce}, and a CC in a fractional density decrease η_{cc}, then

$$N_{cc}(1 - \eta_{cc}) = N_{ce}(\eta_{ce} - 1) - \frac{\Delta V}{\Omega}. \tag{10}$$

3. Ion-induced crystallization and amorphization in U_3Si

Table 1 lists the nominal values of the parameters used in Eqs. (1)–(3a), (3b)–(10) [2].

The kinetics of amorphization are grain-boundary-structure dependent. In Si, the amorphous phase is nucleated heterogeneously at structural defects such as grain boundaries during MeV ion irradiation [19]. Experimental evidence suggests that in Si, self-interstitials are very mobile compared to vacancy motion. Thus, the grain boundary in Si acts as a more efficient sink for interstitials than for

[2] There is no correspondence between many of the variables in this table and Table 1 in Ref. [1], due to the use of dimensionless dependent variables, the utilization of K instead of g (ions/cm^3/s), and a restructuring of terms in Eqs. (1), (4), (6) and (9). Corrections to Table 1 of Ref. [1] are $f_1 = 0.189\Omega^{2/3}$ m^2; $f_2 = 1.31\times10^{-5}\Omega^{2/3}$ m; $f_3 = 2.72\times10^{-18}\Omega^{2/3}$ m^2; $\beta_2 = 0.07$.

Table 1
Values of parameters used in Eqs. (1)–(3a), (3b)–(10) [a]

Parameter	Value	Parameter	Value
N_{ce}	1×10^{-2}	$_a$	1.18 eV
δ	1.67×10^{3} cm^{-1}	$_x$	0.55 eV
f_1	0.1 N_0 cm^{-1}	$_{ie}$	1.4 eV
f_2	10^{-7} N_0 cm^{-1}	η_{ce}	1.3
f_3	1.6×10^{-14} N_0 cm^{-1}	η_{cc}	0.98
v_{cc}	5×10^{5} cm/s	N_0	$\rho a_n / M_w$
β_1	8.4×10^{-3}	V_c	3.35×10^{-20} cm^3
β_2	0.046	$\Delta V/\Omega$	0.02
β_3	5×10^{-7}	$_t$	3 eV
f_{ie}	0.0037	f_t	5×10^{9}
ξ_a	1	ξ_g	1
Ω	N_0^{-1}		

[a] ρ is density, a_n is Avogadro's number, and M_w is molecular weight.

vacancies, leading to an excess concentration of vacancies within a characteristic vacancy diffusion distance of the grain boundary. Amorphous Si is nucleated when the vacancy concentration exceeds a critical value. On the other hand, the results of the analysis presented in this paper leads to the speculation that the grain boundary structure in the intermetallic U_3Si is such that the boundaries act as efficient sinks for vacancies as well as for interstitials.

Fig. 1 shows the calculated and measured temperature dependence of the dose of 1.5 MeV Kr ions, at a flux of 2×10^{12} Kr cm^{-2} s^{-1}, required to amorphize U_3Si ($\rho_{U_3Si_2} = 15$ g/cm^3, $M_w = 742$) with or without high-temperature irradiation treatments. The high-temperature treatments consisted of 1.5 MeV Kr ion irradiation to 5×10^{14} ions/cm^2. Subsequently, the samples were reradiated at the lower temperature. The calculated amorphization dose is based on achieving a close-packed structure of amorphous clusters: spherical entities will touch each other at a fuel volume fraction of about 0.652. The calculated dose follows the trend of the observations and clearly demonstrates the strong effect of grain refinement on ion-beam amorphization: pretreatment raises the amorphization dose and decreases the critical temperature (i.e., the temperature above which the material remains crystalline). The calculated crystallization during the pretreatment at 670 K yields a crystallization volume fraction of about 37% and a crystallized grain diameter of about 50 nm. A high-temperature pretreatment dose of 5×10^{14} Kr cm^{-2} raises the low-temperature amorphization dose by a factor of about 5. Increasing the pretreatment dose by a factor of 2 raises the low-temperature amorphization dose by a factor of at least 40. The calculations are consistent with this observation [1,15].

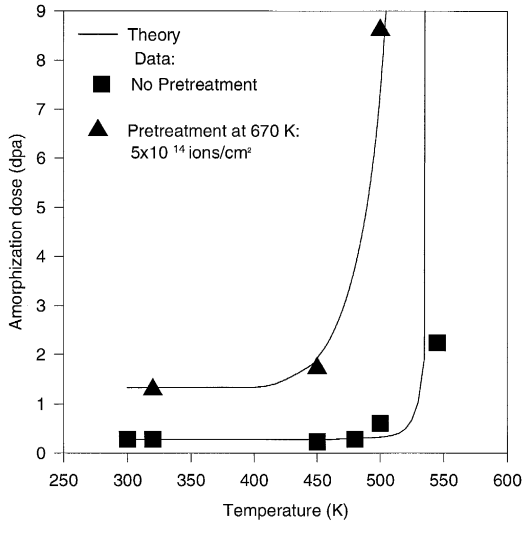

Fig. 1. Calculated and measured temperature dependence of dose of 1.5 MeV Kr ions required to amorphize U_3Si with and without high-temperature irradiation treatments. Increasing the pretreatment dose by a factor of 2 raises the low-temperature amorphization dose by a factor of at least 40. The calculations are consistent with this observation [1,15].

4. Ion-induced amorphization of U_3Si_2

The model was applied to the amorphization of U_3Si_2 ($\rho_{U_3Si_2} = 12$ gm/cm^3; $M_w = 761$) by heavy ions. Fig. 2 shows the calculated and measured temperature dependence of the dose (1.5 MeV Kr ions at a flux of 2×10^{12} Kr cm^{-2} s^{-1}) required to amorphize U_3Si and U_3Si_2 [20]. The calculations show that both U_3Si and U_3Si_2 become amorphous under ion irradiation by about 0.3 dpa. The calculated results for U_3Si_2 were obtained by reducing $_a$

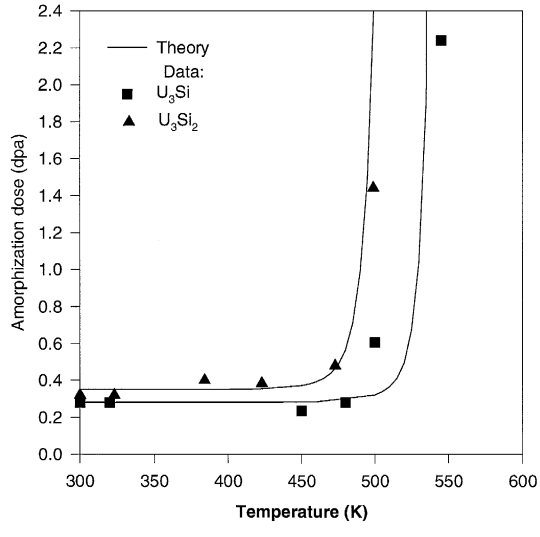

Fig. 2. Calculated and measured temperature dependence of dose of 1.5 MeV Kr ions required to amorphize U_3Si and U_3Si_2.

and $_{ie}$ by 6%, increasing $_{t}$ and $_{x}$ by 6%, and reducing N_{ce} by $\rho_{U_3Si_2}/\rho_{U_3Si}$. The factor of 6% follows the trend of the ratio of the homologous temperatures for the two materials. The value of this ratio is obscured because U_3Si undergoes a phase transformation prior to reaching its melting temperature. In addition, U_3Si expands upon amorphization whereas U_3Si_2 contracts [20]. Although the difference in properties (e.g., energies) between materials is, in general, not directly related to the difference in homologous temperatures, this ratio is used as a guide (e.g., to scale the energies), given the lack of better information. Differences in $_{a}$ and $_{ie}$ between materials are assumed to be proportional to the change in the melting temperature, while differences in $_{t}$ and $_{x}$ are assumed to be inversely proportional. The calculated curves shown in Fig. 2 follow the trend of the observations.

5. Fission-induced amorphization in U_3Si_2

The calculations shown in Figs. 1 and 2 utilize the assumption that full amorphization occurs when the volume fraction of amorphous clusters, C_{ev}, reaches a value of 0.652, the value of the volume fraction at which close-packed spheres just begin to touch. In order to calculate the dose dependence of the amorphous volume fraction, a connection must be established between the density of amorphous clusters and the amorphous volume fraction. The simplest model [21] for the growth of the amorphous volume V_A, can be written as

$$\frac{dV_A}{dKt} = V_i\left(1 - \frac{V_A}{V_O}\right), \tag{11}$$

where it is assumed that in each cascade a sufficiently large defect density is created so that a certain characteristic volume, V_i, is transformed to the amorphous phase. Eq. (11) can be rewritten as

$$\frac{dV_F}{dC_{ev}}\frac{dC_{ev}}{dKt} = V_i(1 - V_F), \tag{12}$$

where

$$V_F = \frac{V_A}{V_O},$$

and using Eq. (1),

$$\frac{dC_{ev}}{dKt} = N_{ce}V_\alpha(1 - C_{ev}). \tag{13}$$

Thus,

$$V_F = 1 - (1 - C_{ev})^x, \tag{14}$$

where

$$x = \frac{V_i}{V_O}\frac{1}{N_{ce}V_\alpha}. \tag{15}$$

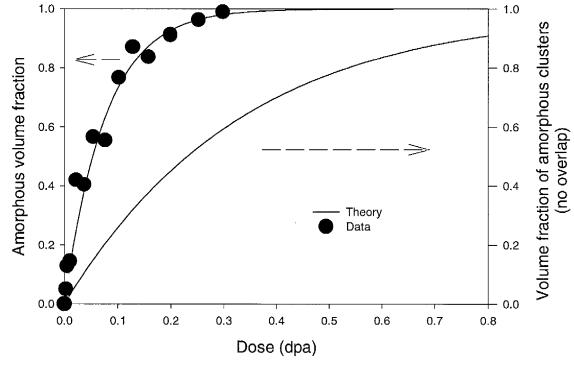

Fig. 3. Calculated and measured amorphous volume fraction during irradiation of U_3Si_2 at 303 K in the IPNS.

Fig. 3 shows the calculated and measured amorphous volume fractions during irradiation of U_3Si_2 at 303 K in the Intense Pulsed Neutron Source (IPNS) at Argonne National Laboratory [20]. Also shown in Fig. 3 is the volume fraction of amorphous clusters, C_{ev}. The value of the ratio $V_i/V_O = (0.076\ \text{dpa})^{-1}$ was taken from Birtcher et al. [20]. The displacement rate, K, in the IPNS is about a factor of 10^{-5} less than during heavy ion irradiation. The calculated amorphous volume fraction of U_3Si_2 follows the trend of the data. Note that full amorphization occurs at the point where the volume fraction of amorphous clusters reaches 0.652 (i.e., the touching of close-packed spheres criterion). The results displayed in Figs. 2 and 3 show that the same amount of damage is required for amorphization of U_3Si_2 by ion or neutron irradiation.

6. Fission-induced recrystallization in UO_2

In this section, fission-induced recrystallization in UO_2 is described in the context of radiation-induced crystallization. The complicated kinetics involved in the formation of a cellular dislocation network (i.e., the observed precursor to recrystallization) are approximated by the formation and growth of subgrains due to the interaction of shock waves produced by fission-induced damage to the UO_2. Before proceeding, it is instructive to review the model for radiation-induced recrystallization described in Ref. [14]. This model is based, in part, on the following assumptions:

- A cellular dislocation structure evolves relatively early in the irradiation period.
- Impurities formed during fissioning of the material diffuse to cell walls as vacancy/impurity complexes. The impurities effectively pin the wall, i.e., dislocation movement to and from the wall is retarded.
- Not all cell walls are uniformly affected by impurities; the walls that contain no impurities continue to undergo subgrain coalescence, which results in viable recrystallization nuclei.

Based on the above discussion, a number C_s of recrystallization nuclei are assumed per unit volume of material. It appears that these nuclei form relatively early in the irradiation period at low values of stored energy and that they are associated with microstructural features such as subgrain-boundary triple points or walls of cellular dislocation structures. Recrystallization nuclei act as sinks for irradiation-produced defects. As the irradiation proceeds, the nuclei are eliminated by interaction with vacancy–solute pairs. In other words, the concentration of impurities reduces the mobility of the interface. Many potential solute atoms are produced during fission, e.g., gas atoms and rare earths. Thus, the available stored energy is concentrated on fewer and fewer nuclei (one can consider that the nuclei are holes in the material and that they act as stress concentrators), with a resultant increase in average energy per nucleus. Recrystallization is induced when the energy per nucleus is high enough to offset the creation of a grain boundary surface by creating a strain-free volume, with a resultant net decrease in the free energy of the material.

It is assumed that the solute atoms require significant energy to become part of a dumbbell-shaped interstitial and therefore do not migrate via an interstitial mechanism. It is further assumed that long-range diffusion of vacancy–solute pairs to the immobile nuclei eliminates the nuclei at a rate given by

$$\frac{\mathrm{d}c_s}{\mathrm{d}t} = -K_{sm} c_s c_m, \tag{16}$$

where c_m is the pair concentration, and K_{sm} (the reaction rate for the immobilization of recrystallization nuclei by vacancy–solute pairs) is defined as

$$K_{sm} = 4\pi r_{sm} D_{vI}/\Omega, \tag{17}$$

where r_{sm} is the annihilation radius of a recrystallization nucleus/vacancy–solute pair, D_{vI} is the diffusivity of the vacancy–solute pair, and Ω is the atomic volume. D_{vI} consists of thermal and athermal components, i.e.,

$$D_{vI} = \xi a^2 \upsilon_v \mathrm{e}^{-\ {}_{vI}/kT} + \chi\sqrt{\dot{f}}, \tag{18}$$

where a is the lattice parameter, υ_v is the vibration frequency factor for vacancies, ${}_{vI}$ is the migration energy for a vacancy–solute pair, ξ is a preexponential factor that accounts for deviations from diffusion in a pure solvent, $\dot{f}$ is the fission rate (fissions/cm^3/s), χ is a factor related to the strength of athermal diffusion, k is Boltzman's constant, and T is the absolute temperature.The concentration of vacancy–solute pairs c_m is given by

$$\frac{\partial c_m}{\partial t} = 12\left(K + 7\omega_4^v c_v\right)c_I - c_m\left(\alpha c_i + 7\omega_3^v\right), \tag{19}$$

where K is the damage rate in displacements per atom per second; c_v and c_i are the concentrations of vacancies and interstitials, respectively; c_I is the solute concentration; ω_3^v and ω_4^v are the jump rates of vacancies away from and toward nearest neighbor nuclei of solute atoms; and α is the recombination coefficient given by

$$\alpha = 12\left(\omega_O^v + \omega_O^i\right), \tag{20}$$

where ω_O^v and ω_O^i are the jump frequencies of vacancies and interstitials, respectively, unperturbed by the presence of a solute atom.

If one assumes [22] that the concentration of vacancy–solute pairs is in steady state with the concentration of vacancies, interstitials, and solute atoms (i.e., $\mathrm{d}C_m/\mathrm{d}t = 0$), the result is

$$12\left(K + 7\omega_4^v c_v\right)c_I = c_m\left(\alpha c_i + 7\omega_3^v\right). \tag{21}$$

This expression for the steady-state concentration of vacancy–solute pairs consists of the direct production of solute-defect pairs by irradiation (first term on the left-hand (LHS) side of Eq. (21)), pair production due to interaction between vacancies and solute atoms (second term on the LHS of Eq. (21)), the loss of pairs through the interaction between vacancy–solute pairs and interstitials (first term on the right-hand side of Eq. (21)), and the loss of pairs due to dissociation (second term on RHS of Eq. (21)). In most cases, direct production of solute–defect pairs by irradiation should have only a small influence on the proportion of vacancies and interstitials trapped in vacancy–solute pairs. However, if the temperature is low, the dose rate is high, and the point-defect–solute binding energy is high, then recombination will be important. For the more general case, where recombination is important, the equation for c_m is obtained from Eq. (21) (neglecting the effect of direct production of vacancy–solute pairs by irradiation, i.e., the first term within parentheses on the RHS of Eq. (21)) as

$$c_m = \frac{84\omega_4^v c_v c_I}{\left(\alpha c_i + 7\omega_3^v\right)}. \tag{22}$$

An equilibrium concentration of mobile defects is reached relatively early in the irradiation. The equilibrium concentration of mobile point defects within the bulk material, c_v and c_i, can be determined from the rate equations that describe point defect behavior, which for negligible bulk diffusion (e.g., to a surface) are given by

$$\frac{\partial c_i}{\partial t} = K - K_{iv} c_i c_v - K_{sv} s_v c_v, \tag{23}$$

and

$$\frac{\partial c_i}{\partial t} = K - K_{iv} c_i c_v - K_{si} s_i c_i, \tag{24}$$

where K_{iv}, K_{sv}, and K_{si} are the rate coefficients for mutual recombination and for the annihilation of vacancies and interstitials at sinks. Here the assumption is made that the overall effect of solute concentration on the steady-state concentration of point defects is small. The sinks, which occupy time-independent fractions of the lattice nuclei, are

assumed to be inexhaustible and randomly distributed. The rate coefficients are

$$K_{iv} = 4\pi r_{iv}(D_i + D_v)/\Omega \cong 4\pi r_{iv} D_i/\Omega, \quad (25)$$

$$K_{sv} = 4\pi r_{sv} D_v/\Omega, \quad (26)$$

$$K_{si} = 4\pi r_{si} D_i/\Omega. \quad (27)$$

Here, r_{iv} is the radius of the recombination volume; r_{sv} and r_{si} are annihilation radii and depend on the type of sink, e.g., dislocation line, jog, or microvoid; and D_v and D_i are the random-walk diffusion coefficients of vacancies and interstitials given by

$$D_v = \xi a^2 \omega_O^v, \quad (28)$$

$$D_i = \frac{2}{3}\xi a^2 \omega_O^i, \quad (29)$$

where ξ is a preexponential factor that accounts for deviations from diffusion in a pure solvent,

$$\omega_O^v = \upsilon_v e^{-\ v/kT}, \quad (30)$$

and

$$\omega_O^i = \upsilon_i e^{-\ i/kT}, \quad (31)$$

where, $_v$, $_i$ and υ_v, υ_i are the migration energies and vibration frequency factors for vacancies and interstitials, respectively.

When one uses Eqs. (17), (20) and (21) in Eq. (16), and because $\omega_O^v \ll \omega_O^i$, the result is

$$\frac{1}{c_s}\frac{dc_s}{dt} = -\frac{28\pi r_{sm} c_I D_{vI} \omega_4^v c_v}{\Omega\left(c_i + 7\omega_3^v/12\,\omega_O^i\right)\omega_O^i}. \quad (32)$$

The concentration of viable recrystallization nuclei, which results from the integration of Eq. (32), is quite different from that given by classical nucleation theory in that the concentration decreases with fluence instead of increasing with irradiation, until the nucleation barrier is surmounted and the higher energy state of the crystal forms. In the present case, the nuclei are formed early in the irradiation by the damage process at relatively low values of strain energy. As the irradiation proceeds and the nuclei are eliminated by interaction with the vacancy–solute pairs, the available stored energy is concentrated in fewer and fewer nuclei, thus increasing the energy per nucleus.

Recrystallization is induced when the energy per nucleus is high enough that the creation of grain-boundary surfaces is offset by the creation of strain-free volumes, with a resultant net decrease in the free energy of the material. The stored energy, E_s, is taken to be concentrated in the network, c_s. In the theory of the nucleation of liquid droplets in a vapor [24], the condition for equilibrium is that the net change in the free energy ΔG_m be a minimum. From this condition and assuming that the number of single molecules/volume $\gg$ number of clusters/volume the equilibrium number of clusters c_s is found to be

$$c_s = c_s^O \exp[-\Delta G_s/kT], \quad (33)$$

where ΔG_s is the minimum standard free energy of formation of a cluster. A cluster containing just i^*, the critical number of molecules is called a nucleus. A cluster smaller than the nucleus will, on the average, completely dissociate after a time since its standard free energy increases with the addition of molecules. However, a cluster containing more than i^* molecules will continue to grow, on the average (and become a domain of the new phase), since its standard free energy is continuously decreased. Thus, to become a nucleus, a cluster must acquire (by growing to critical size) a critical standard free energy ΔG^* in excess of that of single vapor molecules. From the above equation, the equilibrium number of nuclei c_s^* per unit volume is

$$c_s^* = c_s^O \exp[-\Delta G^*/kT]. \quad (34)$$

Differentiating this equation with respect to c_*^s:

$$1 = -\frac{c_s^*}{kT}\frac{d\Delta G^*}{dc_s^*}, \quad (35)$$

or

$$\frac{d\Delta G^*}{dc_s^*} = -\frac{kT}{c_s^*}. \quad (36)$$

By equating c_s obtained from Eq. (32) to the value of c_s obtained from Eq. (36) where a relatively small energy fluctuation can allow the system to jump over the energy barrier and cause the creation of a relatively defect-free crystal of material, a relation for the value of the fission density, FDX (m^{-3}) at which recrystallization will occur is obtained [14,23]

$$FDX = \frac{E_{sf}\left[9\Omega\dot{f} + 7a\sqrt{\pi B r_{iv}\xi\upsilon_v\Omega\dot{f}}\,e^{-(\ vI - \ v/2)/kT}\right]}{168\pi r_{sm} kTc_I\left(\xi_{vi}a^2\upsilon_v e^{-\ vI/kT} + \chi_2\dot{f}\right)}, \quad (37)$$

where $E_{sf} = E_s + \Delta G^*$.

Nevertheless, this physical picture of the processes leading up to recrystallization (e.g., evolution of a cellular dislocation structure) is qualitative and has eluded a mechanistic description. An interesting supposition is whether an alternative description of the evolution of the recrystallization nuclei can be obtained with the theory of irradiation-induced amorphization and crystallization described in Section 2. To apply this model to UO_2, the same methodology is used as that used to determine U_3Si_2 properties from those used for U_3Si: $_a$ and $_{ie}$ were decreased by the ratio of the melting temperature of U_3Si_2 and UO_2, $_t$ and $_x$ were increased by the ratio of the melting temperature, and N_{ce} was reduced by $\rho_{UO_2}/\rho_{U_3Si_2}$. In addition, it is assumed that for UO_2, the amorphus clusters formed in

the damage cascades are very unstable and quickly crystallize, i.e., $\xi_a = 10^{-9}$, and $\xi_g = 5 \times 10^{-4}$. This value for ξ_a is consistent with ion irradiation data that shows that UO_2 remains crystalline at 20 K [25].

Fig. 4 shows the calculated grain density and grain diameter using Eqs. (1)–(3a), (3b)–(10) as a function of fission density for an irradiation at 623 K and an average fission rate of 1×10^{13} fissions/cm^3/s. The calculated grain density peaks relatively early in the irradiation period. Also shown in Fig. 4 is the concentration of viable recrystallization nuclei, C_s, which results from the integration of Eq. (32). Comparing C_s with the calculated grain density confirms the interpretation that these nuclei form relatively early in the irradiation period at low values of stored energy and that they are associated with microstructural features such as subgrain-boundary triple points or walls of cellular dislocation structures. It is clear from Fig. 4 that subsequent to the initial buildup of crystallized grains, C_s follows the trend of the calculated density of crystallized grains obtained from the solution of Eqs. (1)–(3a), (3b)–(10). In addition, the behavior of the calculated crystallized grain diameter as a function of burnup is consistent with the observations reported by Nogita and Une [13,26]: that low-angle boundaries begin to form above $\approx 7.5 \times 10^{20}$ fissions/cm^3 (indicated by a circled 1 in Fig. 4), and that subdivided grains 20–30 nm in size and recrystallized grains 50–200 nm in size adjacent to the subdivided grains exist in fuel irradiated to about 2×10^{27} fissions/m^3 (indicated by a circled 3 in Fig. 4). The theory of radiation-induced recrystallization (i.e., Eq. (36) which is given by the intersection of Eqs. (32) and (35) predicts that recrystallization is initiated at $\approx 1.5 \times 10^{21}$ fissions/cm^3 (indicated by a circled 2 in Fig. 4). Recrystallization is predicted to occur at a slightly larger dose by the intersection of Eqs. (6) and (35).

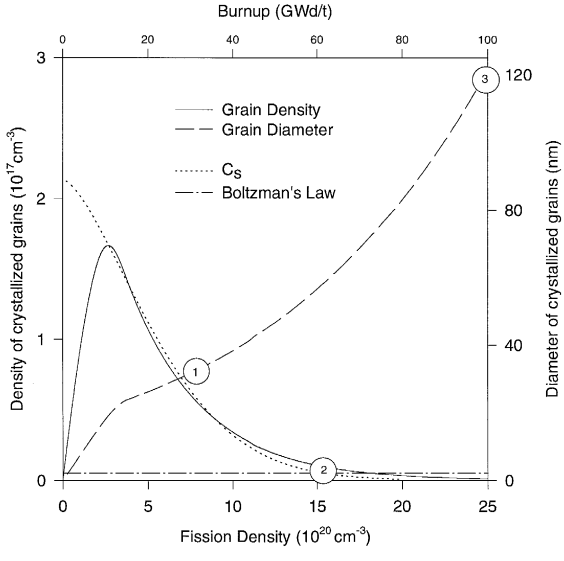

Fig. 4. Calculated grain density and grain diameter using Eqs. (1)–(3a), (3b)–(10) as a function of fission density for irradiation at 623 K and average fission rate of 1×10^{13} fissions/cm^3/s. Also shown in Fig. 4 is concentration of viable recrystallization nuclei, C_s, which results from integration of Eq. (32). Observations reported by Nogita and Une [13,26]: low-angle boundaries begin to form above $\approx 7.5 \times 10^{20}$ fissions/cm^3 (indicated by a circled 1), and subdivided grains 20–30 nm in size and recrystallized grains 50–200 nm in size exist in fuel irradiated to $\approx 2 \times 10^{21}$ fissions/cm^3 (indicated by a circled 3). Prediction of the theory of radiation-induced recrystallization (i.e., Eq. (36) given by the intersection of Eqs. (32) and (35)), that recrystallization is initiated at $\approx 1.5 \times 10^{21}$ fissions/cm^3, is indicated by a circled 2. Recrystallization is predicted to occur at a slightly larger dose by the intersection of Eqs. (6) and (35).

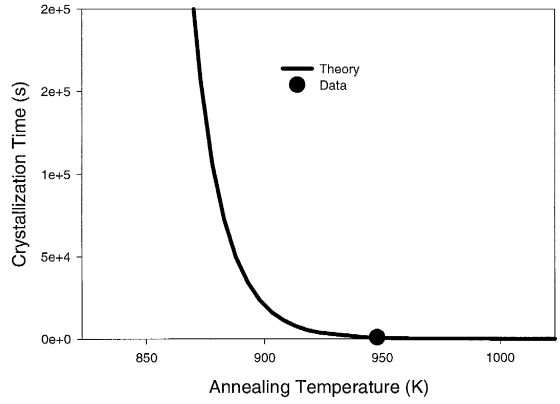

Fig. 5. Calculated time to achieve crystallization of amorphous UO_2 as a function of annealing temperature compared with data of Ref. [27].

Fig. 5 shows the calculated time to achieve crystallization of amorphous UO_2 as a function of the annealing temperature compared with the data of Ref. [27]. Evaporation of bulk UO_2 during electron-beam heating led to the condensation of amorphous UO_2 films. The substrates were amorphous carbon films kept at ambient temperature. As is seen from Fig. 5, the results of the theory described in Section 2 applied to UO_2 are consistent with the experimental result that the UO_2 films recrystallized at $T_c = 675 \pm 15$°C, as verified by electron diffraction.

7. Discussion

An estimate of the cell size of a cellular dislocation structure evolved from shock-wave interaction can be obtained from a consideration of the limited range of energies at which a damage event may be able to create a great enough density of fast recoils to form a shock wave [6]. For uranium ions in uranium, the maximum energy transfer is about 0.5 keV and occurs at an energy of about 4 keV. If one assumes that this energy transfer goes into creating dislocation loops having a radius equal to the

Burgers vector, then in UO_2 a CC interaction will produce about 15 loops. Coalescence of these loops into a cubic cellular configuration results in a cell size of about 2 nm.

The values of the rate constants f_1–f_3 and the parameters β_1–β_3 are somewhat arbitrary. In principle, these constants could be evaluated in the context of generalizing the present model to include interaction with radiation-produced defects. However, such an evaluation is outside the scope of the present work. The methodology of value determination for various model parameters used in Eqs. (1)–(3a), (3b)–(10) is based on a qualitative representation of the phenomenology. For example, the value of V_α was set by the amorphization dose at 300 K (no preconditioning); β_1 and f_1 were set by the asymptotic radius of recrystallized grains at the end of high-temperature irradiation; β_2 and f_2 were set by the volume fraction of recrystallized grains at the end of high-temperature irradiation; β_3 and f_3 were set by the low-T slope of amorphization dpa versus T (no preconditioning); $_a$ was set by the critical temperature; $_t$ was set such that V_O^f decreases above the critical temperature, and such that the calculation is consistent with the measured amorphization dose just below the critical temperature; δ was set by the slope of amorphization dpa versus T for irradiation of preconditioned material: its value is constrained by the condition that grain radius and volume fraction show asymptotic behavior.

The number of unknown materials properties and parameters used in the model are listed in Table 1. In all there are 21 unknown materials properties and parameters. However, the calculations are not strongly dependent on all of these parameters (for example, the calculations are not strongly dependent on the velocity of a shock wave, taken to be the velocity of an acoustic wave in the solid, as well as on the value of $\Delta V/\Omega$, or on the values of η_{ce} and η_{cc}). The treated and untreated U_3Si irradiation consists of 10 data points; the ion and neutron irradiated U_3Si_2 consists of 20 data points; the annealing experiment on UO_2 and the observation of UO_2 recrystallization consist of two data points — for a total of 32 data points — substantially more than the '17' unknown materials properties and parameters used in the model. The model has also been able to calculate the observed recrystallization during Kr irradiation of U_3Si above the critical temperature for amorphization (see Ref. [1]). In addition, the model has been applied to the dose-rate and temperature dependent ion-induced motion of the interface between crystalline and amorphous phases of U_3Si and these predictions have been 'successfully' compared to data and results of calculations for ion bombardment of Si (see Ref. [1]). The key point here is that only 7 of the 21 materials properties and parameters in the model were altered (and in a methodical, physical manner) in order to describe all three materials investigated, i.e., U_3Si, U_3Si_2, and UO_2.

The present model has a wider applicability than other models based on direct amorphization including or not cascade superposition [8,21,28,29] in that it provides information on the evolution of the amorphous cluster and crystallized grain size distribution. In addition, it not only provides an interpretation of the ion-induced motion of the crystalline/amorphous interface in Si, and a prediction for this process in U_3Si [1], but provides an interpretation of the experiments on the ion-induced nanocrystallization and amorphization of U_3Si and U_3Si_2 [15,20] as well as recrystallization in UO_2.

The key finding that amorphization of a crystallized U_3Si grain is hindered by the presence of the grain boundary is supported by data [15], but is in contrast to work in Si where it was shown that the amorphous phase is nucleated heterogeneously at structural defects such as grain boundaries during MeV ion irradiation [19]. However, the kinetics of amorphization are grain boundary structure dependent. Experimental evidence suggests that in Si self-interstitials are very mobile compared to vacancy motion. Thus, the grain boundary in Si acts as a more efficient sink for interstitials than for vacancies, leading to an excess concentration of vacancies within a characteristic vacancy diffusion distance of the grain boundary. Amorphous Si is nucleated when the vacancy concentration exceeds a critical value. On the other hand, in other materials the grain boundary acts as an efficient sink for vacancies. For example, it is well know that in materials such as UO_2, the grain boundaries are an efficient sink for vacancies; gas bubbles on the grain boundaries grow at an accelerated rate as compared to those in the bulk material. We speculate here that the grain boundary structure in U_3Si is such that the boundaries of the recrystallized grains act as efficient sinks for vacancies as well as for interstitials.

An alternative mechanism for the evolution of recrystallization nuclei is described for a model of irradiation-induced recrystallization of UO_2 wherein the stored energy in the UO_2 is concentrated in a network of sinklike nuclei that diminish with dose due to interaction with radiation-produced defects. The sinklike nuclei are identified as cellular dislocation structures that evolve relatively early in the irradiation period. A generalized theory of radiation-induced amorphization and crystallization, developed for uranium silicide, is applied to UO_2. The complicated kinetics involved in the formation of a cellular dislocation network are approximated by the formation and growth of subgrains due to the interaction of shock waves produced by fission-induced damage to the UO_2. Unlike U_3Si and U_3Si_2, where crystallized grain nuclei are formed primarily by the annihilation of amorphous clusters by shock waves, recrystallization nuclei in UO_2 are formed by the interaction between shock waves. CC annihilation upon contact form either oriented or slightly disoriented crystal structures. This process is also present in the intermetallics, but at a much reduced level as compared to that provided by CC–CE annihilation.

In the more 'stable' UO_2, amorphous clusters do not survive cascade 'cooling.' It is possible that a crystallized

region is formed in the wake of cascade solidification, but this would lead to very high crystallization rates (in U_3Si, nanocrystals are formed above the critical temperature for amorphization at a rate of about one per ion [15]), leading to saturation of the material with nanocrystals within several tenths of a dpa. In this case, in order to explain the evolution of the dislocation and subgrain structure reported in Ref. [26], a mechanism of nanocrystal destruction would have to be postulated which would be strong enough to delay the filling of space with crystallized material from several dpa to thousands of dpa. Observations of UO_2 irradiated at room temperature with 500 keV Xe ions to 10^{16} ions/cm^2 are not consistent with this mechanism [25]. Instead, the observations show an increased dislocation density and the presence of small subgrains separated with the edges of the dislocations. Thus, within the context of the model presented in this paper, it seems plausible to postulate that the primary mechanism available to form recrystallized grain nuclei is CC–CC annihilation.

References

[1] J. Rest, J. Nucl. Mater. 225 (1995) 308.
[2] M. Guinan, J. Nucl. Mater. 53 (1974) 171.
[3] Y. Hayashiuchi, Y. Kitazoe, T. Sekiya and Y. Yamamura, J. Nucl. Mater. 71 (1977) 181.
[4] Y. Kitazoe and Y. Yamamura, Radiat. Eff. Lett. 50 (1980) 39.
[5] G. Carter, Radiat. Eff. Lett. 50 (1980) 105.
[6] K.W. Winterbon, Radiat. Eff. Lett. 57 (1980) 89.
[7] V.P. Zhukov and A.V. Ryabenko, Radiat. Eff. 82 (1984) 85.
[8] C. Jaouen, Solid State Phenom. 23&24 (1992) 123.
[9] N.E. Cunningham, M.D. Freshley and D.D. Lanning, J. Nucl. Mater. 188 (1992) 19.
[10] T. Kameyama, T. Matsumura and M. Kinoshita, Proc. ANS Topical Meeting on LWR Fuel Performance, Avignon, France (1991) p. 620.
[11] K. Une, K. Nogita, S. Kashibe and M. Imamura, J. Nucl. Mater. 188 (1992) 65.
[12] L.E. Thomas, C.E. Beyer and L.A. Charlot, J. Nucl. Mater. 188 (1992) 80.
[13] K. Nogita and K. Une, Nucl. Instrum. Methods B91 (1994) 301.
[14] J. Rest and G.L. Hofman, J. Nucl. Mater. 210 (1994) 187.
[15] R.C. Birtcher and L.M. Wang, Mater. Res. Soc. Symp. Proc. 235 (1992) 467.
[16] L.M. Wang, R.C. Birtcher and R.C. Ewing, Nucl. Instrum. Methods. B80&81 (1993) 1109.
[17] R.J. White and M.O. Tucker, J. Nucl. Mater. 118 (1983) 1.
[18] J. Rest and A.W. Cronenberg, J. Nucl. Mater. 168 (1989) 243.
[19] H.A. Atwater and W.L. Brown, Appl. Phys. Lett. 56 (1990) 30.
[20] R.C. Birtcher, J.W. Richardson and M.H. Mueller, J. Nucl. Mater. 230 (1996) 158.
[21] D.M. Parkin and R.O. Elliott, Nucl. Instrum. Methods B16 (1986) 193.
[22] S.M. Murphy, J. Nucl. Mater. 168 (1989) 31.
[23] J. Rest and G.L. Hofman, J. Nucl. Mater. 223 (1995) 192.
[24] D. Turnbull, in: Solid State Physics, eds. F. Seitz and D. Turnbull, Vol. 3 (Academic Press, New York, 1956) p. 226.
[25] L.M. Wang and Hj. Matzke, J. Nucl. Mater. (1996) to be published.
[26] K. Nogita and K. Une, J. Nucl. Mater. 226 (1995) 302.
[27] Hj. Matzke, V. Nitzki and C. Ronchi, Thin Solid Films 22 (1974) 75.
[28] K.A. Jackson, J. Mater. Res. 3 (1988) 1218.
[29] E.P. Simonen, Nucl. Instrum. Methods B16 (1986) 198.